Current Applied Physics 20 (2020) 331–336

Contents lists available at ScienceDirect

Current Applied Physics

journal homepage: www.elsevier.com/locate/cap

Dual-band isotropic metamaterial absorber based on near-field interaction in the Ku band

The Linh Pham[a], Hong Tiep Dinh[a], Dinh Hai Le[a], Xuan Khuyen Bui[b], Son Tung Bui[b], Hong Luu Dang[a], Anh Duc Phan[c], Dac Tuyen Le[d,**], Dinh Lam Vu[a,b,*]

[a] Graduate University of Science and Technology, Vietnam Academy of Science and Technology, 18 Hoang Quoc Viet, Hanoi, Viet Nam
[b] Institute of Materials Science, Vietnam Academy of Science and Technology, 18 Hoang Quoc Viet, Hanoi, Viet Nam
[c] Phenikaa Institute for Advanced Study, Artificial Intelligence Laboratory, Faculty of Information Technology, Materials Science and Engineering, Phenikaa University, Hanoi 12116, Vietnam
[d] Department of Physics, Hanoi University of Mining and Geology, 18 Pho Vien, Hanoi, Viet Nam

ARTICLE INFO

Keywords:
Metamaterials
Isotropic absorber
Perfect absorption
Near-field coupling

ABSTRACT

We numerically and experimentally investigate single-band and dual-band isotropic metamaterial absorbers (IMAs) based on metallic disks. By optimizing the diameter of the metallic disks and the thickness of the dielectric substrate, the single-band IMA is observed at 16.2 GHz with absorptivity of 97%. When adding one disk-pair to the structure, the dual-band IMA is obtained at 12.8 and 15.5 GHz due to the symmetry breaking. The physical mechanics is explained by near-field coupling effect and equivalent LC circuit model. The measurement results performed in the range 12–18 GHz show a good agreement with simulation and theoretical analysis. Our findings demonstrate a new approach to achieve dual-band and multi-band IMAs.

1. Introduction

Great advances in metamaterials (MMs) have offered revolutionary devices and applications since they are artificial materials having extraordinary electromagnetic features not found in nature. The first theoretical analysis of metamaterials was introduced by Veselago 50 years ago [1] while the first MM design was experimentally demonstrated by Pendry et al. [2,3] and Smith et al. [4] in the year of 90s. So far, several noticeable applications have been developed by exploiting MM, such as sensor [5], antenna [6], and particularly perfect absorbers [7–11]. Despite much scientific effort devoted to designing and optimizing MM structures to achieve desired properties over five decades, some problems still remain especially the operation bandwidth, which is limited by the electromagnetic resonance nature of MM.

Metamaterial perfect absorbers (MPAs) with the desired frequency have been drawing significant attention due to their primary contributions to military science and technological engineering such as optical switches [12], bolometers [13], and energy harvester [14]. The MPA concept was introduced the first time in 2008 by Landy et al. [7]. It indicates that the electric permittivity and magnetic permeability can be tailored to suppress the reflection and the transmission simultaneously. Afterwards, various structures of MPAs have been proposed and studied in different frequency ranges from MHz to the visible regime [15–22]. In a common structure, MPA has three layers, the front layer is patterned structure and the back layer is continuous metallic film, that makes the anisotropic absorption. Therefore, several structures were exploited to obtain isotropic absorption [23,24]. In 2013, Gu et al. presented the planar isotropic broadband metamaterial absorber by using dendritic structure with extremely complicated geometry [23]. To simplify a complication of the geometrical design, another isotropic metamaterial absorber (IMA) was proposed by creating a superposition of the magnetic and electric resonances in 2015 [24]. However, this approach is difficult to create dual-band absorption because of limitation of narrow electromagnetic resonance.

In this work, we demonstrate the structures for IMA to obtain a single-band and dual-band in the range of frequency from 12 to 18 GHz, or the so-called Ku band. Firstly, the absorbers are systematically investigated by simulation, and the absorption behavior is understood via equivalent LC circuit. Then, the samples are fabricated and the absorption spectra are measured, that verify the good performance of the proposed IMAs.

* Corresponding author. Graduate University of Science and Technology, Vietnam Academy of Science and Technology, 18 Hoang Quoc Viet, Hanoi, Viet Nam.
** Corresponding author.
E-mail addresses: ledactuyen@humg.edu.vn (D.T. Le), lamvd@ims.vast.ac.vn (D.L. Vu).

https://doi.org/10.1016/j.cap.2019.11.024
Received 28 December 2018; Received in revised form 1 October 2019; Accepted 30 November 2019
Available online 02 December 2019

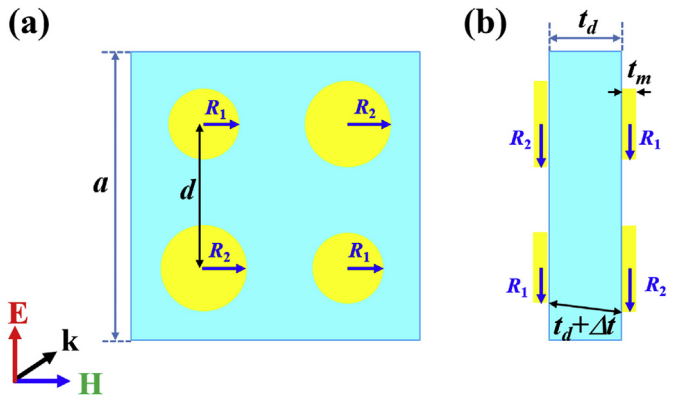

Fig. 1. Schematic representation of the IMA structure with the polarization of electromagnetic wave: (a) top view and (b) side view. a = 18 mm, t_d = 0.4 mm, t_m = 0.036 mm, R_1 and R_2 are disk radii, d is distance between two proximal disks.

2. Design, simulation, and experiment

Fig. 1 illustrates the unit-cell design of the proposed IMA structure with periodicity a = 18 mm. The FR-4 dielectric substrate is sandwiched between the top and the bottom layers that are made of copper disks. As shown in Fig. 1a, four disks are located at the center of the quadrantal parts of the unit-cell. At the other side of FR-4 substrate, four disks are also opposite as shown in Fig. 1b. The FR-4 substrate has permittivity of 4.3, loss tangent of 0.025, and thickness of t_d = 0.4 mm [25–27]. The copper disks have conductivity of 5.96 × 10^7 S/m, thickness of t_m = 0.036 mm, and radii indicated as R_1 and R_2. The distance between centers of two proximal metal disks in the same plane is d.

The numerical simulation was performed using the finite integration method by the Computer Simulation Technology (CST) Microwave Studio [28]. The polarized compositions and the propagation direction of incident electromagnetic wave are shown in Fig. 1, where (**E, H**) plane is parallel to the top view of the IMA structure and the propagation vector ***k*** is normal. The absorption is calculated through the scattering parameters by equation $A(\omega) = 1 - |S_{11}|^2 - |S_{21}|^2$, where S_{11} and S_{21} are reflection and transmission coefficients, respectively [29].

The typical samples were fabricated by using mask photolithography technique. A printed circuit board consists of 0.4 mm-thick FR-4 substrate sandwiched between two 0.036 mm-thick copper layers. Firstly, both sides of the printed circuit board are coated with photoresist layer, then covered by patterned masks of designed structure. After exposure processes, wet-etching was used to remove copper film, resulting the structural pattern. The measurement was carried out using a Keysight Fieldfox N9918A microwave vector network analyzer, which is connected to linearly-polarized microwave standard-gain horn antennas to obtain results of reflection and transmission.

3. Results and discussion

3.1. Optimization for single-band isotropic metamaterial perfect absorber

Fig. 2a shows the absorption spectra of the proposed IMA structure with radii R_1 = R_2 = 2.4 mm and different distances d = 8, 9, and 10 mm for our basic IMA. In case of d = 9 mm, the copper disks place in the center of four quadrants, and the distance between two closest disks are equal. It is clearly observed that all the absorption spectra have one resonant peak located at around 16.9 GHz with the absorptivity of 49%. The result is expected since the symmetry leads to an equality of interactions on each component. The structure is simplified and equivalent to a disk at the center of the unit-cell periodicity of 9 mm. As shown in Fig. 2b, the electric field distribution reveals that the absorption peak at 16.9 GHz is associated with the magnetic resonance [30,31]. This absorption frequency can be approximately calculated by

$$f_m = \frac{1}{2\pi\sqrt{L_m C_m}} \quad (1)$$

where L_m and C_m are effective values of inductor and capacitor at magnetic resonance frequency, respectively, which are computed in previous work [32]. Analytical expressions of L_m and C_m are

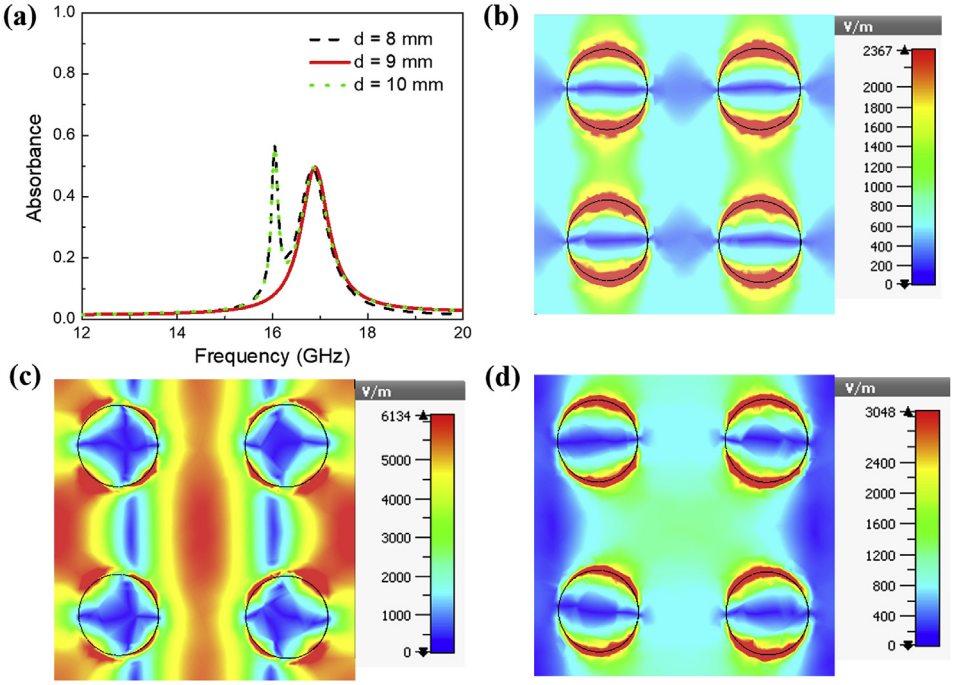

Fig. 2. (a) Simulated absorption spectra of proposed IMA structure with various values of d. (b) Distribution of electric field at 16.9 GHz in case of d = 9 mm. (c) and (d) Distribution of electric field at 16.2 and 16.9 GHz in case of d = 10 mm, respectively.

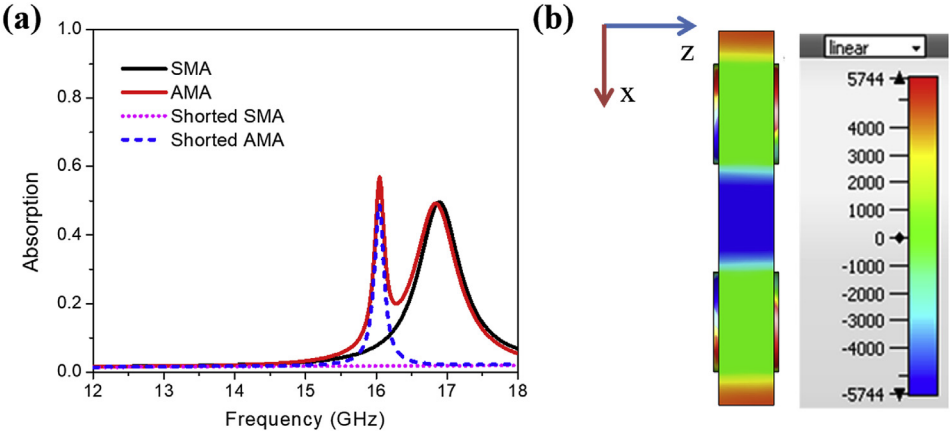

Fig. 3. (a) Absorption spectra of original and shorted versions of asymmetric (AMA) and symmetric (SMA) structures (b) Electric-field distribution at 16.2 GHz in (X, Z) plane.

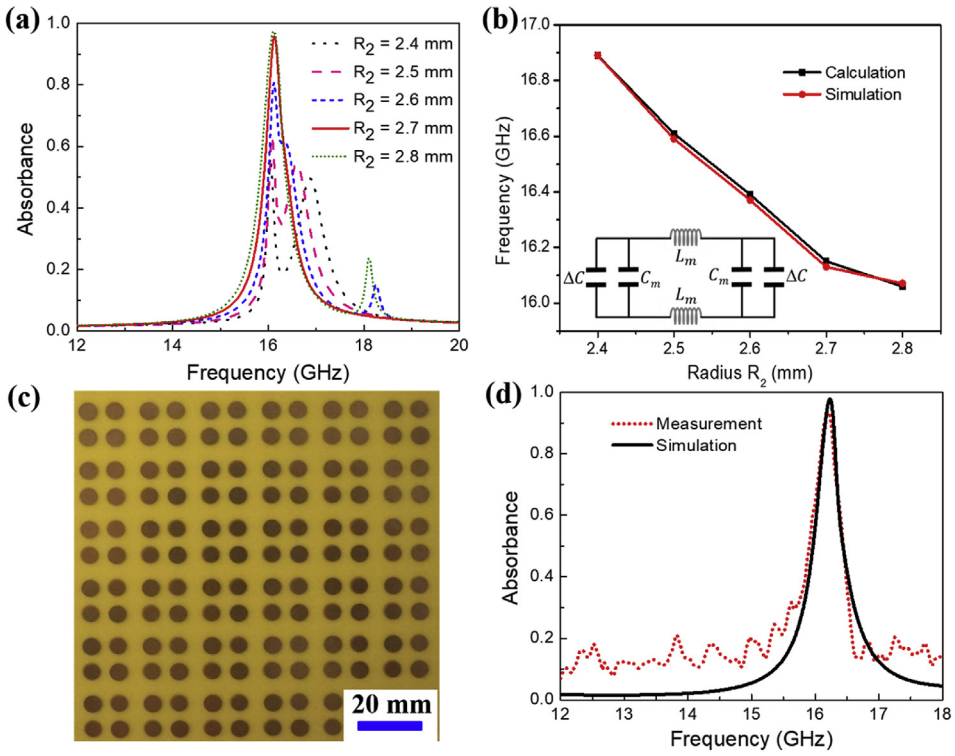

Fig. 4. (a) The dependence of absorption on the values of R_2 in the Ku band, (b) Simulated and calculated absorption frequencies according to the R_2. The inset is the equivalent LC circuit model. (c) Prototype of the IMA structure in case of R_1 = 2.4 mm, R_2 = 2.7 mm and d = 10 mm. (d) Simulated and measured absorption spectra of the single-peak IMA.

$$L_m = \mu\mu_0(2t_m + t_d)\,\pi/2 \text{ and } C_m = \varepsilon\varepsilon_0 c_1 \pi {R_1}^2/(2t_d), \quad (2)$$

where ε and μ are the permittivity and permeability of the dielectric substrate, respectively. ε_0 is the vacuum permittivity, μ_0 is the vacuum permeability, and c_1 is the ratio of the charge distribution area to the disk area. When c_1 = 0.11, the calculated absorption frequency is 16.9 GHz, in good agreement with the simulated result. This finding indicates that the resonant peak at 16.9 GHz is attributed to all the disks as the fundamental magnetic resonance of the structure.

When the distance d is set to be 8 and 10 mm, an additional peak is observed at located around 16.2 GHz. It is caused by interactions between each other disks because the geometrical structure is asymmetric. Fig. 2c and d shows the electric field distribution at the 16.2 and 16.9 GHz in the case of d = 10 mm, respectively. In Fig. 2d, the electric field concentrates at the similar positions to its in Fig. 2b. It confirms the fundamental magnetic resonance at 16.9 GHz. While, in Fig. 2c for 16.2 GHz, the electric field mostly concentrates at space between adjacent disks. This result indicates the coupling interaction between the adjacent disks and the resonant peak at 16.2 GHz is attributed to coupled resonances. To understand the physical mechanism, we consider the near-field coupling effect [33], which is also well known as the electromagnetically induced transparency [34]. When distance d is various, the geometrical symmetry of the IMA structure is broken and the initial unit-cell can be visualized as a 4-disk group. Thus, the periodicity of initial structure increases by two times, in the same order of operating wavelength and the obtained resonance is due to guided mode resonance of 2-D metallic grating structure [35–37].

In order to justify the assumption, we investigate the electromagnetic resonance of both shorted symmetric and asymmetric absorber (SMA and AMA) structures. We add metallic wires connecting disk-pairs from both sides to remove the effective capacitors, then the fundamental magnetic resonance (16.9 GHz) is disappeared in both case of shorted symmetric metamaterial absorbers (shorted SMA) and shorted asymmetric metamaterial absorbers (shorted AMA) as shown in Fig. 3a. However, the shorted AMA structure still has the coupled resonance (16.2 GHz) due to near-field coupling resonance of disk-pairs

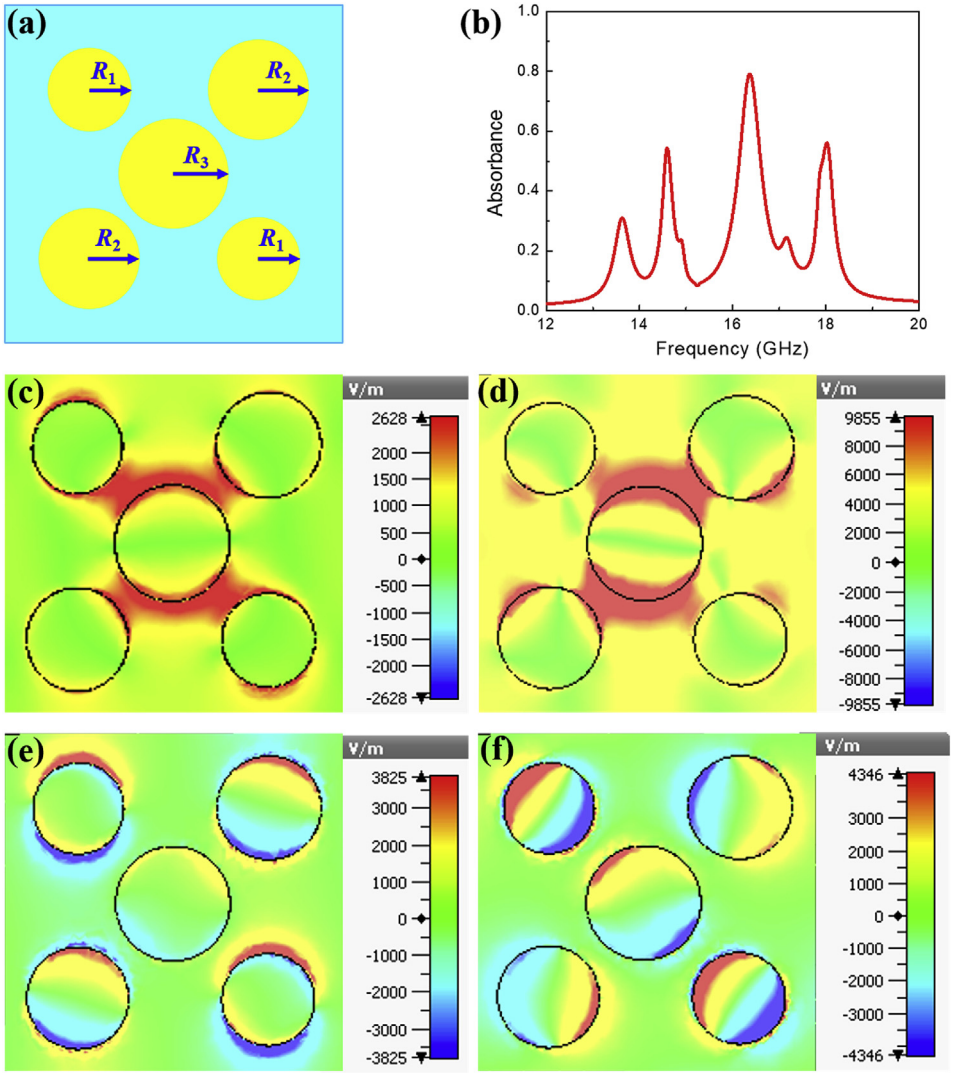

Fig. 5. (a) Top view of the unit-cell of the proposed dual-band IMA, (b) Simulated absorption spectrum of the proposed dual-band IMA, (c)–(f) The electric field distribution of resonant peaks at 13.6, 14.6, 16.4 and 18.0 GHz, respectively.

structure. While shorted SMA structure is not observed this resonance. These results confirm that the proposed AMA structure exhibits both the magnetic and near-field resonances. Fig. 3b indicates that all localized magnetic resonances are suppressed in the (X, Z) plane. Consequently, the guided mode resonance is responsible for the existing resonance.

Changing structural parameter easily tunes the fundamental absorption frequency and our goal is to superpose two resonances. By manipulating the geometrical size of two diagonal opposite disks, the magnetic resonance frequency shifts to a lower frequency and superposes with the raised peak. The overlapping leads to a perfect absorption at the raised peak frequency. Fig. 4a shows how the absorption depends on the radius R_2. Our results indicate that we have achieved the single-band isotropic perfect absorption at $R_2 = 2.7$ mm since the two peaks are completely overlapped with absorptivity of 97%. In order to understand the influence of the radius R_2 on the fundamental resonance, we use the effectively equivalent LC circuit model for one disk-pair in the top (radius R_1) and bottom layers (radius R_2) as shown in Fig. 4b. When $R_2 > R_1$, the effective distance between two capacitors is increased from $t = t_d + 2t_m$ to $t' = [t^2 + (R_1 - R_2)^2]^{1/2}$. A growth of the total capacitance from C_m to $C_m = C_m + \Delta C$ causes a slight reduction of the magnetic frequency. More accurately, the effective capacitance and the magnetic resonant frequency are respectively formulated by

$$C_m' = \frac{2\varepsilon\varepsilon_0 c_1 R_1^2 R_2^2}{(R_1^2 + R_2^2)\sqrt{t^2 + (R_1 - R_2)^2}},$$
$$f_m' = \frac{c\sqrt{(R_1^2 + R_2^2)[t^2 + (R_1 - R_2)^2]^{1/2}}}{2\pi R_1 R_2 \sqrt{\mu\varepsilon c_1 t\pi}}, \quad (3)$$

where c is the speed of light. By using Eq. (3), the frequency value f_m' is calculated as a function of R_2. In the case of $d = 10$ mm, the calculated frequencies are coincident with simulation results, as shown in Fig. 4b for $f_m' = 16.9$ GHz with $c_1 = 0.21$ and $f_m' = 16.2$ GHz with $c_1 = 0.25$. The geometrical factor c_1 is in agreement with the range from 0.05 to 0.3 [30].

To verify the numerical results, we fabricate the prototype IMA following our design with the values $R_1 = 2.4$, $R_2 = 2.7$ and $d = 10$ mm, as illustrated in Fig. 4c. The absorption is 93.5% at 16.2 GHz in measurement, as shown in Fig. 4d, which indicates a good agreement between experiment and simulation. Our theoretical analysis also confirms that the main experimental absorption peak was obtained by superposing both fundamental resonance and coupling mode.

3.2. Improvement in dual-band isotropic metamaterial absorber

Based on the results in the previous subsection, we extend the design of the basic IMA to achieve dual-band IMA. From the coupled

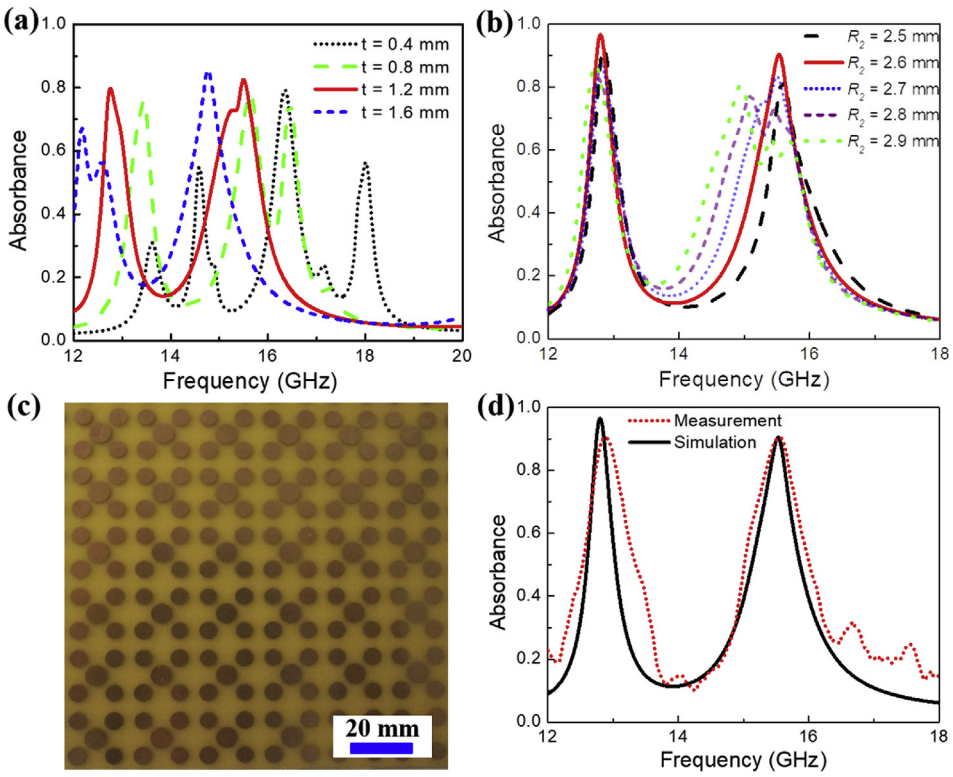

Fig. 6. (a) The dependence of absorption on thickness t_d of FR-4 layer. (b) The dependence of absorption on radius R_2 when $R_1 = 2.4$, $R_3 = 3.0$ and $t_d = 1.2$ mm. (c) Prototype of proposed dual-band IMA structure with $R_1 = 2.4$, $R_2 = 2.6$, $R_3 = 3.0$ and $t_d = 1.2$ mm. (d) Comparison of simulation (black line) and measurement (red dash line). (For interpretation of the references to colour in this figure legend, the reader is referred to the Web version of this article.)

resonances in the single-band IMA, we expect that adding one disk-pair of radius $R_3 = 3$ mm to both sides of the unit cell as in Fig. 1a reduces the distance between in-plane disks and therefore enhances the coupling effect. To remain symmetry, a pair of additional disks are located at the center of the unit-cell. The top view and the simulated absorption spectrum of the dual-band IMA are exhibited in Fig. 5a and b, respectively. Clearly, the appearance of the added disk-pair excites the near-field coupling modes and induces indirect coupling effect via the central disk. It results in four pronounced absorption peaks at 13.6, 14.6, 16.4 and 18.0 GHz. Fig. 5c-f shows the electric field distribution of those resonances from low to high frequency, respectively. In Fig. 5c and d, the electric field concentrates mostly around the central disk, which indicated that the first and the second peaks are associated with the central disk and coupling interaction between the central disk and the adjacent disks. On the other hand, the electric field distributions of the third and the fourth resonance frequencies strongly focus on the outer disks.

In order to superpose those peaks, the thickness of FR-4 dielectric substrate is varied from 0.4 to 1.6 mm. As observed in Fig. 6a, an increase of t_d leads to the overlapping between resonances. When thickness t_d is changed from 0.4 to 1.2 mm, the first and second peaks are superposed and the third and fourth peaks are overlapped. Many interesting features can be seen in the absorption spectrum of $t_d = 1.2$ mm. There two main peaks at 12.8 and 15.5 GHz when the thickness t_d is 1.2 mm. The absorption amplitudes at these two distinct resonance frequencies are relatively the same. The absorption peak at 15.2 GHz can be considered as a shoulder for that at 15.5 GHz. However, the overlapping between two frequency bands at 15.2 and 15.5 GHz is not perfect. To improve the perfection, we fix $t_d = 1.2$ mm and change R_2 to see how the absorption spectrum varies in Fig. 6b. The two resonance peaks located at around 15.5 GHz are shifted according to the change of R_2, while the resonance peak at 12.8 GHz is nearly unchanged. When the radius value of R_2 is 2.6 mm, the dual-band IMA is obtained at 12.8 and 15.5 GHz with absorptivity of 96% and 90%, respectively.

To validate the numerically result, we fabricate the prototype of the dual-band IMA and measure its absorption spectrum. In case of $t_d = 1.2$ mm, Fig. 6c presents a photo of the sample with radii $R_1 = 2.4$, $R_2 = 2.6$ and $R_3 = 3.0$ mm. An agreement between simulation and experiment is achieved in Fig. 6d, where the absorption peaks are located at 12.88 and 15.56 GHz with an absorption of 90.5% and 90.3%, respectively. The small discrepancy in spectrum shape between simulated and experimental results might be due to the error in the fabrication process. In detail, the photolithography technique makes the disk-pair structures to be ununiform and inexactly coaxial (on both sides of the fabricated sample).

4. Conclusion

We have demonstrated an efficient method to generate single-band and dual-band IMA in the Ku band frequency. Firstly, the single-band IMA is obtained by asymmetric structure when the fundamental magnetic resonance superposes on coupled resonance at 16.2 GHz with absorptivity of 97%. The equivalent LC circuit model is used to confirm resonant frequency and to understand the underlying physical mechanism. For further improvement, one disk-pair is added to the structure, the dual-band IMA can be achieved at around 12.8 and 15.5 GHz with absorptivity over 90%. The experimental results are consistent with simulation and theoretical analysis. Our work is expected to unlock a new simple and effective approach for the next generation of the multi-band IMAs.

Acknowledgements

This research is funded by Vietnam National Foundation for Science and Technology Development (NAFOSTED) under grant number 103.02-2017.67.

References

[1] V.G. Veselago, The electrodynamics of substances with simultaneously negative values of ε and μ, Sov. Phys. Uspekhi 105 (1968) 509, https://doi.org/10.1070/PU1968v010n04ABEH003699.

[2] J.B. Pendry, A.J. Holden, W.J. Stewart, I. Youngs, Extremely low frequency plasmons in metallic mesostructures, Phys. Rev. Lett. 76 (1996) 4773, https://doi.org/10.1103/PhysRevLett.76.4773.
[3] J.B. Pendry, A.J. Holden, D.J. Robbins, W.J. Stewart, Magnetism from conductors and enhanced nonlinear phenomena, IEEE Trans. Microw. Theory Tech. 47 (1999) 2075, https://doi.org/10.1109/22.798002.
[4] D.R. Smith, W.J. Padilla, D.C. Vier, S.C. NematNasser, S. Schultz, Composite medium with simultaneously negative permeability and permittivity, Phys. Rev. Lett. 84 (2000) 4184, https://doi.org/10.1103/PhysRevLett.84.4184.
[5] T.S. Bui, T.D. Dao, L.H. Dang, L.D. Vu, A. Ohi, T. Nabatame, Y.P. Lee, T. Nagao, C.V. Hoang, Metamaterial enhanced vibrational ab-sorption spectroscopy for the detection of protein molecules, Sci. Rep. 6 (2016) 32123, https://doi.org/10.1038/srep32123.
[6] J. Hao, L. Zhou, M. Qiu, Nearly total absorption of light and heat generation by plasmonic metamaterials, Phys. Rev. B 83 (2011) 165107, https://doi.org/10.1103/PhysRevB.83.165107.
[7] N.I. Landy, S. Sajuyigbe, J.J. Mock, D.R. Smith, W.J. Padilla, Perfect metamaterial absorber, Phys. Rev. Lett. 100 (2008) 207402, https://doi.org/10.1103/PhysRevLett.100.207402.
[8] A. Moreau, C. Cirac, J.J. Mock, R.T. Hill, Q. Wang, B.J. Wiley, A. Chilkoti, D.R. Smith, Controlled-reflectance surfaces with film-coupled colloidal nanoantennas, Nature 492 (2012) 86–89, https://doi.org/10.1038/nature11615.
[9] L.D. Hai, V.D. Qui, D.H. Tiep, P. Hai, T.T. Giang, T.M. Cuong, B.S. Tung, V.D. Lam, Dual-band perfect absorption by breaking the symmetry of metamaterial structure, J. Electron. Mater. 46 (2017) 3757, https://doi.org/10.1007/s11664-017-5333-z.
[10] K. Aydin, V.E. Ferry, R.M. Briggs, H.A. Atwater, Broadband polarization-independent resonant light absorption using ultrathin plasmonic super absorbers, Nat. Commun. 2 (2011) 517, https://doi.org/10.1038/ncomms1528.
[11] L.D. Hai, V.D. Qui, N.H. Tung, T.V. Huynh, N.D. Dung, N.T. Binh, L.D. Tuyen, V.D. Lam, Conductive polymer for ultra-broadband, wide-angle, and polarization-insensitive metamaterial perfect absorber, Opt. Express 26 (2018) 33253, https://doi.org/10.1364/OE.26.033253.
[12] H.T. Chen, W.J. Padilla, J.M.O. Zide, S.R. Bank, A.C. Gossard, A.J. Taylor, R.D. Averitt, Ultrafast optical switching of terahertz metamaterials fabricated on ErAs/GaAs nanoisland superlattices, Opt. Lett. 32 (2007) 1620, https://doi.org/10.1364/OL.32.001620.
[13] F.B.P. Niesler, J.K. Gansel, S. Fischbach, M. Wegener, Metamaterial metal-based bolometers, Appl. Phys. Lett. 100 (2012) 203508, https://doi.org/10.1063/1.4714741.
[14] T.S. Almoneef, O.M. Ramahi, Metamaterial electromagnetic energy harvester with near unity efficiency, Appl. Phys. Lett. 106 (2015) 153902, https://doi.org/10.1063/1.4916232.
[15] B.X. Khuyen, B.S. Tung, Y.J. Yoo, Y.J. Kim, V.D. Lam, J.G. Yang, Y.P. Lee, Ultrathin metamaterial-based perfect absorbers for VHF and THz bands, Curr. Appl. Phys. 16 (2016) 1009, https://doi.org/10.1016/j.cap.2016.05.027.
[16] Y.J. Kim, J.S. Hwang, Y.J. Yoo, B.X. Khuyen, X. Chen, Y.P. Lee, Triple-band metamaterial absorber based on single resonator, Curr. Appl. Phys. 17 (2017) 1260, https://doi.org/10.1016/j.cap.2017.06.009.
[17] M. Tonouchi, Cutting-edge terahertz technology, Nat. Photonics 1 (2007) 97, https://doi.org/10.1038/nphoton.2007.3.
[18] W. Wang, Y. Qu, K. Du, S. Bai, J. Tian, M. Pan, H. Ye, M. Qiu, Q. Li, Broadband optical absorption based on single-sized metal-dielectric-metal plasmonic nanostructures with high-ε″ metals, Appl. Phys. Lett. 110 (2017) 101101, https://doi.org/10.1063/1.4977860.
[19] F. Ding, J. Dai, Y. Chen, J. Zhu, Y. Jin, S.I. Bozhevolnyi, Broadband near-infrared metamaterial absorbers utilizing highly lossy metals, Sci. Rep. 6 (2016) 39445, https://doi.org/10.1038/srep39445.
[20] H. Li, L.H. Yuan, B. Zhou, X.P. Shen, Q. Cheng, T.J. Cui, Ultrathin multiband gigahertz metamaterial absorbers, J. Appl. Phys. 110 (2011) 014909, , https://doi.org/10.1063/1.3608246.
[21] M.-H. Li, H.-L. Yang, X.-W. Hou, Y. Tian, D.-Y. Hou, Perfect metamaterial absorber with dual bands, Prog. Electromagn. Res. 108 (2010) 37–49, https://doi.org/10.2528/PIER10071409.
[22] D. Kundu, A. Mohan, A. Chakrabarty, Single layer wideband microwave absorber using array of crossed dipoles, IEEE Antennas Wirel. Propag. Lett. 15 (2016) 1589, https://doi.org/10.1109/LAWP.2016.2517663.
[23] S. Gu, B. Su, X. Zhao, Planar isotropic broadband metamaterial absorber, J. Appl. Phys. 114 (2013) 163702, https://doi.org/10.1063/1.4826911.
[24] D.T. Viet, N.V. Hieu, V.D. Lam, N.T. Tung, Isotropic metamaterial absorber using cut-wire-pair structures, APEX 8 (2015) 032001, , https://doi.org/10.7567/APEX.8.032001.
[25] L. Stephen, N. Yogesh, V. Subramanian, Realization of bidirectional, bandwidth-enhanced metamaterial absorber for microwave applications, Sci. Rep. 9 (2019) 10058, https://doi.org/10.1038/s41598-019-46464-6.
[26] C. Ji, C. Huang, X. Zhang, J. Yang, J. Song, X. Luo, Broadband low-scattering metasurface using a combination of phase cancellation and absorption mechanisms, Opt. Express 27 (2019) 23368–23377, https://doi.org/10.1364/OE.27.023368.
[27] E. Ahamed, M.M. Hasan, M.R.I. Faruque, M.F.B. Mansor, S. Abdullah, M.T. Islam, Left-handed metamaterial inspired by joint TD geometry on flexible $NiAl_2O_4$ substrate, PLoS One 13 (6) (2018) e0199150, , https://doi.org/10.1371/journal.pone.0199150.
[28] CST Microwave Studio: A Numerical Simulation Software for Electromagnetic Computing, Computer Simulation Technology GmbH, Darmstadt, Germany. https://www.cst.com.
[29] H.T. Chen, Interference theory of metamaterial perfect absorber, Opt. Express 20 (2012) 7165, https://doi.org/10.1364/OE.20.007165.
[30] J. Zhou, E.N. Economon, T. Koschny, C.M. Soukoulis, Unifying approach to left-handed material design, Opt. Lett. 31 (2006) 3620, https://doi.org/10.1364/OL.31.003620.
[31] D.T. Viet, N.T. Hien, P.V. Tuong, N.Q. Minh, P.T. Trang, L.N. Le, Y.P. Lee, V.D. Lam, Perfect absorber metamaterials: peak, multi-band and broadband absorption, Opt. Commun. 322 (2014) 209, https://doi.org/10.1016/j.optcom.2014.02.037.
[32] D.H. Luu, N.V. Cuong, L.D. Hai, N.H. Tung, N.V. Dung, T.M. Cuong, L. D Tuyen, V.D. Lam, Broadband metamaterial perfect absorber obtained by coupling effect, J. Nonlinear Opt. Phys. Mater. 26 (2017) 1750036, https://doi.org/10.1142/S0218863517500369.
[33] B.S. Tung, B.X. Khuyen, Y.J. Kim, V.D. Lam, K.W. Kim, Y.P. Lee, Polarization-independent, wide-incident-angle and dual-band per-fect absorption, based on near-field coupling in a symmetric metamaterial, Sci. Rep. 7 (2017) 11507, https://doi.org/10.1038/s41598-017-11824-7.
[34] S. Zhang, D.A. Genov, Y. Wang, M. Liu, X. Zhang, Plasmon induced transparency in metamaterials, Phys. Rev. Lett. 101 (2008) 047401, , https://doi.org/10.1103/PhysRevLett.101.047401.
[35] H. Chen, J. Liu, Z. Hong, Guided mode resonance with extremely high q-factors in terahertz metamaterials, Opt. Commun. 383 (2017) 508512, https://doi.org/10.1016/j.optcom.2016.09.042.
[36] Y. Sun, H. Chen, X. Li, Z. Hong, Electromagnetically induced transparency in planar metamaterials based on guided mode resonance, Opt. Commun. 392 (2017) 142, https://doi.org/10.1016/j.optcom.2017.01.046.
[37] D.H. Luu, B.S. Tung, B.X. Khuyen, L.D. Tuyen, V.D. Lam, Multi-band absorption induced by near-field coupling and defects in metamaterial, Optik 156 (2018) 811, https://doi.org/10.1016/j.ijleo.2017.12.025.